Two-Component Systems in Human Cells: A Basic Look at LOV And Hno Pathways for Tool Development To Advance Immunotherapy

By

DIANA SERNAS

DISSERTATION

Submitted in partial satisfaction of the requirements for the degree of

DOCTOR OF PHILOSOPHY

in

Integrative Genetics and Genomics

in the

OFFICE OF GRADUATE STUDIES

of the

UNIVERSITY OF CALIFORNIA

DAVIS

Approved:

Sean R. Collins, Chair

Becky Parales

Cheemang Tan

Committee in Charge

2024

Abstract

Our immune system responds to extracellular cues to protect our health by coordinating necessary cell functions from cell motility to apoptosis. Engineering signaling pathways controlling these processes is rapidly becoming a powerful approach for developing new biomedical technology, with cancer immunotherapies serving as a prominent example. However, most current strategies rely on modifying or repurposing endogenous human signaling cascades. This can result in unintended crosstalk between the synthetic signaling pathways and the complex native signaling of human cells. Two-component systems (TCS) could address this challenge and establish a scientific foundation for systematically improving and adding to the natural abilities of cells to sense and respond to their environment in a robust yet flexible manner. With a newly paved avenue for engineering cell communication, researchers could develop strategic signaling cascades in any human cell for their specific research interests. Importantly, TCS are absent in human cells, but present in all three domains of life, and offer diverse yet simple and linear signaling pathways. In TCS, ligand binding modulates a histidine kinase (HK) sensor, a protein characteristically containing separate ligand binding and HK domains. When activated, the HK transfers a phosphoryl group to the response regulator (RR), and the phosphorylated RR activates a specific downstream response through mechanisms ranging from protein-to-protein interactions to transcription. In its inactive state, the HK acts as a phosphatase. These studies focus on a light-sensitive LOV TCS and a nitric oxide-sensitive Hno TCS as candidate model pathways for modifying mammalian cells. We demonstrated constitutive activity with the LOV pathway and tested several modifications to achieve light sensitivity. While some modifications affected pathway output, all tested pathways appeared to have light-independent constitutive activity.

Table of Contents

Chapter 1

Introduction: two-component systems engineered into human cells for synthetic signaling

Diana Sernas

Department of Microbiology and Molecular Genetics, University of California, Davis, Davis, CA, USA.

1.1 Preface

This chapter provides an overview of the relevant background information related to the work presented here. Section 1.2 provides an overview of the current state of cell-based therapies, including their potential and challenges. In section 1.3, there is a general overview of the molecular biology of two-component systems in their native organisms. Section 1.4 describes the current state of how TCS have been implemented in mammalian systems. Finally, section 1.5 emphasizes how TCS can help address challenges laid out in the prior section 1.2 and a brief overview of how we sought to utilize TCS.

1.2 Cell-based therapies: immunotherapies

Cell-based therapies (CBT) have shown exciting potential to address blood cancers that have failed traditional treatments. An exciting and prominent example is chimeric antigen receptor (CAR) T-cells, which have demonstrated amazing success with blood cancers in multiple clinical trials (1–3). CAR T-cells are genetically engineered cells expressing a receptor on the cell surface to recognize a particular surface marker. Upon binding its target, the receptor activates endogenous T-cell signaling pathways which results in killing of the target cell. The

B-cell marker CD19 has been used extensively as a surface marker for hematological malignancies (2,4). However, the progress of CAR T-cells for treating solid tumors has been limited due to challenges including difficulties in identifying tumor specific surface markers and a limited ability of the cells to penetrate solid tumors (1,2,4). The use of markers shared between tumors and healthy cells, leaves healthy cells at risk of "on-target off-tumor effects" (2).

Major advances in cell-based immunotherapies emerge from strong foundational work in synthetic biology (5). For instance, the current design of CARs is based on basic research conducted, at least since 1989, regarding single-chain variable fragments of antibodies and native T-cell signaling pathways (4). This work eventually led to CARs with selected targets for therapeutic applications. In addition to CARs, the landscape of therapeutic strategies has been expanded through the development of synthetic Notch (synNotch) receptors (6,7). synNotch receptors are engineered with modular extracellular domains that can be switched to make receptors capable of sensing the specific signal of interest (7). These receptors were developed based on detailed understanding of the function of the naturally occurring Notch family of receptors.

To overcome the limitations of a single cell surface marker, researchers are now developing more complicated strategies to integrate inputs from multiple receptors. CARs are sensitive to a decrease in expression of the antigen of interest, and thus strategies are being developed based on introduction of multiple CARs into a single cell (8). synNotch receptors can be engineered to have tumor specific signaling domains and can be used in combination with other receptors in logic-gate networks (9). Both strategies implementing a combination of receptors advance CBT by addressing precision targeting of tumor cells to minimize off-target effects.

Currently, CBTs for cancer face multiple roadblocks including antigen heterogeneity within tumors, immunosuppressive tumor microenvironments, and limited homing and infiltration of solid tumors. To help overcome these roadblocks, we set out to produce new, robust yet flexible tools for cell engineering that will lead to advances in immunotherapies. We focused on short, simple pathways that could be easily adapted for different outputs or for logic-based circuits.

1.3 Two-Component Systems

Two-component systems (TCS) offer a promising framework to pave a new avenue for advancing immunotherapies. TCS offers modular short signaling networks with a variety of sensors that use a biochemically distinctive phosphotransfer mechanism.

TCS are ubiquitous signaling pathways found in bacteria and observed across the evolutionary tree from fungi to plants, but absent in mammalian cells (5,6). TCS can act as a basic intracellular rheostat signaling mechanism allowing organisms to readily sense, respond, and adapt to changes in environmental cues (10–12). These systems are characterized by their highly modular design including a histidine kinase sensor (HK) protein, containing separate ligand binding and histidine kinase domains, and a response regulator (RR) protein, with a regulatory domain (11). Ligand binding modulates HK activities. When activated the HK transfers a phosphoryl group to the RR, and the phosphorylated-RR (p-RR) activates a specified downstream response. In many cases, phosphorylation of the RR causes it to bind to DNA, where it activates or represses transcription (10,11). However, other pathways work through phosphorylation-dependent binding of the RR to effector proteins, or through RR

oligomerization. Importantly, in its inactive state the HK acts as a phosphatase, which means that the positive and negative regulation in the pathway is encoded in a single protein (10,13,14).

Adapting TCS to develop new synthetic sensing pathways for cell engineering has great potential for overcoming challenges in CBT. TCS offers a variety of features that cellular engineers can take advantage of. First, TCS includes short and well-characterized networks across all domains of life, meaning that there are sensors for diverse inputs (10). In contrast to CARs and synNotch receptors, TCS can respond to extracellular or intracellular signals, including small soluble molecules. Thus, they expand the landscape of what can be detected for downstream applications in medicine or repurposing in basic research. Secondly, because TCS has not been observed in mammalian cells (10), this should result in minimal crosstalk with endogenous networks. Lastly, TCS outputs are diverse from transcriptional regulation to protein-protein interactions (10), thus expanding the possible phenotypes researchers can engineer for cells of interest. While others have tried to implement TCS pathways in mammalian cells, no one has yet been successful (13,15).

1.4 State of TCS in mammalian cell systems

Prior studies have shown partial success in transplanting bacterial TCS pathways into mammalian cells. However, the resulting pathways were constitutively active and lacked responsiveness to the receptor's ligand (13). In particular, Hansen *et al.* transiently expressed engineered variants of three different bacterial TCS pathways in HEK293 cells. They chose the EnvZ-OmpR, NarXL, and DcuSR pathways, which are among the best studied TCS pathways in *E. coli*. In each case, their design included fusing the pathway's RR to the VP16 mammalian transcriptional activation domain. They measured fluorescence to track transcriptional output for

their TCS. The results showed production of the reporter gene if and only if both the HK and RR were present in the same cell, but the results did not depend on the presence of the ligand (13).

These results demonstrate that an HK can phosphorylate an RR and cause it to activate the transcription of a reporter gene. Despite lacking ligand-sensitivity, the demonstrated ability of an HK to catalyze phosphotransfer serves as important proof-of-principle for engineering TCS gene circuits into mammalian cells, since the His-Asp phosphorylations use a different molecular mechanism than Ser/Thr/Tyr phosphorylations (10). These results suggest the possibility of creating a new family of signaling pathways with a diverse array of sensors that use an orthogonal phosphochemical transfer mechanism to the dominant form in eukaryotes (13,15).

I introduced the same Nar pathway components as used in prior studies and verified that we observe constitutive activity as previously reported (13). Reproducing these results confirmed that both the RR-transcriptional activator and the synthetic promoter work.

In conclusion, there has been progress in integrating TCS in mammalian cells, however, the field still faces challenges for utilizing transmembrane sensors. In our preliminary results reproducing prior work, we failed to achieve proper and consistent membrane localization of HKs. We also observed punctate localization across the cytosol for several HKs. It is possible that improper folding of the HKs led to this punctate localization. Therefore, we pivoted our focus to TCS that harness the capabilities of cytoplasmic HKs, while simultaneously testing different receptor inputs.

1.5 Advancing TCS in mammalian cell systems

We set out to develop TCS as a general platform for engineering new sensing pathways in mammalian cells and to overcome challenges that limited previous studies. Such studies were

partially successful with TCS with sensors that localized on the cell surface (13); however, because the sensors were only partially localized to the cell outer membrane and appeared to be constitutively active, we focused on TCS that utilized sensors that localized in the cytosol of the cell. Thus, we bypassed the potential barrier that comes with differences between bacterial membranes and the mammalian plasma membrane. Additionally, we focused our studies on systems that are sensitive to light or nitric oxide. We chose these stimuli because of the ease to control their exposure for the cells in our experiments. Lastly, prior studies introduced all components using transient expression, which can lead to high and variable expression levels (13,15). Thus, we sought to test if stable genomic integration of each component can help establish ligand-sensitivity and perhaps improve the reproducibility of results.

To reach higher levels of transcriptional activity, we tested a more efficient transcriptional activator, VPR, rather than VP16 and VP64 which were used in earlier studies (13). VPR was systematically tested in comparison to other activators in dCas9 fusions in human cells, and shown to significantly improve levels of activation in comparison to dCas9-VP64 (16). VPR is a fusion of VP64 and two additional transcription activators, p65 and Rta (16). This results in a larger construct, which may have contributed to the challenges for the introduction and stable expression of RRs.

We tested genomic integration of the genes of interest to make stable HEK293 cell lines instead of using transient transfection to promote more consistent gene expression levels across cells. We tagged sensors with a fluorescent protein, mCherry, to monitor their localization. Similarly, we tagged RRs with mTurquiose2 to analyze their localization throughout the cell. We codon optimized all constructs for human cells. Furthermore, we added nuclear import and export sequences to RRs to aid transportation across the mammalian nuclear membrane.

Chapter 2

LOV in mammalian cells: Mutations reduce basal activity but remain unresponsive to light

Diana Sernas, Aditi Thambala, Alex Calderon, Sabrina Truoung, Sarah Sun, Shashank Shastry, Sean R. Collins

Department of Microbiology and Molecular Genetics, University of California, Davis, Davis, CA, USA.

2.1 Preface

This chapter describes how we tested and characterized the LOV TCS pathway from *Brucella abortus* in HEK293 cells. Section 2.2 provides the rationale for choosing LOV for proof-of-principle experimentation, a review of how the components in the TCS behave in their native environments, and an overview of how the LOV TCS was adapted for integration and testing in human cells. In section 2.3, there is a summary of the results demonstrating that the LOV pathway is light-independent in mammalian cells, with varying HK versions. Section 2.4 provides an interpretation of the results and the limitations of the experiments executed. Section 2.5 provides a brief summary of the design and molecular cloning of each of the components used, creation of stable cell lines, and transfection of cells for experiments where applicable. Lastly, section 2.6 contains the accumulated figures referenced to throughout Chapter 2.

2.2 Introduction

LOV pathway as a model cytoplasmic TCS for cell engineering

We selected the LOVhk pathway because it utilizes a cytoplasmic sensing kinase, and is sensitive to light, which is easy to monitor and control during experiments. We hypothesized that utilizing cytoplasmic sensors would bypass the previous challenges with improper transmembrane sensor subcellular localization. The Collins Lab has also acquired a decade of experience in developing, testing, and imaging other light-responsive proteins. Additionally, in contrast to the more common TCS output of transcription, this pathway readout involves a protein-protein interaction. This alternative output could be adapted by researchers for a broad variety of engineering applications based on protein recruitment or other protein-protein interactions of interest.

LOV pathway in bacteria

There are diverse HKs across the many organisms with TCS including photosensory HKs, and from photosensory domains, LOV domains are among the best characterized (17). In the bacterial pathogen *B. abortus*, the LOV domain-containing sensor LOVhk plays a role in regulating host-pathogen interactions in a range of mammalian cell types, through activation of the response regulator, PhyR (18). LOVhk quickly and specifically phosphorylates PhyR, but at a lower amount than is typical for cognate component pairs in *B. abortus* (18). PhyR regulates transcription, but does so in a way contrary to the typical mechanisms in TCS that involve binding of the RR directly to DNA (10). Instead, when PhyR is phosphorylated (p-PhyR), it increases its affinity for the anti-sigma factor NepR (18). NepR regulates transcription by

binding and inhibiting a sigma factor (Fig. 1a). When NepR is bound to p-PhyR, the complex releases the sigma factor, which allows it to activate transcription (18) (Fig. 1b).

The LOVhk from the pathogenic bacterium *B. abortus* contains three domains, from N to C terminus, including a LOV domain, a PAS (Per-Arnt-Sin) domain, and a histidine kinase domain (Fig. 2a) (19). LOVhk is sensitive to blue light due to the presence of the LOV domain, as is the case for many other LOV domain containing proteins (18–20). The PAS domain has been experimentally shown to respond to something other than blue light and is hypothesized to detect oxidative stress (18). The N-terminal helix following the LOV domain has been demonstrated to promote parallel dimer formation (20). Like other LOV domains, the LOV domain in LOVhk binds a flavin chromophore, which gets covalently linked to a cysteine residue in the LOV domain in response to stimulation by blue light. This cysteine is required for a broader light-dependent conformational change in the structure of the LOVhk dimer, which activates the kinase (19,20).

LOV domain primary structures exhibit high conservation across diverse organisms (19). The LOVhk protein in *B. abortus* contains protein domains similar to those in the LOV domain observed in LOVhk of *Brucella melitensis*, suggesting that they may exhibit similar active states (19). Affinity assays conducted on purified full-length protein expressed in *E. coli* demonstrated that the *B. melitensis* LOV domain remains in its active state for over 2 hours before returning to the ground state in darkness (19). This stability contrasts that of many other LOV domain-containing proteins, which on average revert to their ground state in darkness after approximately 27 minutes (19). The rate at which the LOV domain reverts to its inactive state regulates the inactivation process following light-induced activation. Through mutational analyses of the LOV domain, studies identified mutations that either accelerate or decelerate this

reversion rate (17). In particular, the V416L mutation in the *A. sativa* LOV2 domain decelerated the reversion rate by approximately two orders of magnitude (17). In contrast, the V416T mutation in *A. sativa* accelerated the reversion rate by about 20-fold (17).

Typically, HK proteins mediate both phosphorylation and dephosphorylation activity in TCS; however, the amino acid residues required for catalyzing these distinct reactions are not the same (10). In the NarXL TCS of *E. coli*, which has been extensively studied, the histidine kinase NarX autophosphorylates at His-399. This residue is responsible for the phosphotransfer, but is not required for phosphatase activity (21). Experimental studies demonstrated that a histidine-to-glutamine (H to Q) mutation at this site in NarX resulted in a protein that only demonstrated phosphatase activity (21).

Although LOVhk, PhyR, and NepR appear to comprise a well-defined light-responsive pathway in *B. abortus*, another protein named LovR has been observed to interact with the pathway. LovR is a single-receiver domain RR that lacks an output domain and interacts with LOVhk (22). Studies demonstrated that in a similar LOV TCS from *Erythrobacter litoralis* also contains an analogous LovR, LovR can be phosphorylated by LOVhk, and it can promote dephosphorylation of PhyR in vitro. Based on these results, LovR was hypothesized to act as a phosphate-sink promoting phosphate turnover which could rapidly deactivate PhyR (23).

LOV pathway adapted for mammalian cells

Our strategy harnessed the regulated binding between PhyR and NepR to use localization as alternate output rather than transcription. A shift in protein subcellular localization is faster than a transcriptional response, and therefore it should be easier to detect upon turning off the

TCS. Because protein relocation can be used to control a variety of different cellular processes, such as signal transduction, this system provides opportunities for future engineering approaches.

To adapt the *B. abortus* LOV pathway for use in mammalian cells, we engineered NepR with a nuclear localization sequence (NLS) on its C-terminus. Therefore, NepR was expected to localize primarily to the nucleus and retain its ability to interact with PhyR (Fig.1c). PhyR was expected to be readily able to access both the cytoplasm and the nucleus due to its small size of only 264 amino acids. Finally, p-PhyR was expected to induce binding to NepR, and binding was anticipated to keep PhyR in the nucleus (Fig.1d).

To test different switch-off rates of the LOVhk sensory protein, we identified the *B. abortus* protein possessed a leucine (L) at the position corresponding to the mutation responsible for decelerating the reversion rate in the *A. sativa* protein. This observation suggested that substituting leucine with threonine (T) in the sequence could potentially result in a significant alteration in the switch-off rate. Therefore, we designed a mutated LOVhk by introducing a leucine-to-threonine (L to T) substitution, specifically L35T (Fig. 2c).

To enhance phosphatase activity in the LOV TCS within human cells, we engineered a version of the HK with both LOV and PAS domains deleted to eliminate sensing capabilities, while also introducing a H288Q mutation (Fig. 2d). Histidine-288 in the LOVhk of *B. abortus* was identified as the phosphorylation site of this sensory protein (18). This construct is later referred to as LovQ. As an alternative approach to increase phosphatase activity, we tried expressing LovR.

2.3 Results

Wild-type LOVhk from B. abortus is sufficient to activate downstream responses independently of light stimulation

Our general strategy tested the activity and light responsiveness of the pathway using live cell imaging experiments. To verify the expression and localization of each two-component system (TCS) component, we fused each component with a fluorescent protein at the C-terminus. Each fluorescent protein was chosen to ensure spectral compatibility, avoiding overlap in their excitation ranges: PhyR-mScarlet-I, HK-mTurqoiuse2, NepR-iRFP670. To establish a baseline, we captured red fluorescent protein (RFP) images reflecting PhyR localization prior to blue light exposure, as imaging the cyan fluorescent protein (CFP) was anticipated to stimulate LOVhk. All subsequent images constituted a time course for the response to light. Finally, to count the number of cells in a given frame and verify the nucleus of each cell, all cells were stained with an ultraviolet (UV) nuclear dye. To test the responsiveness of the *B. Abortus* LOV pathway in HEK293 cells, we expressed the wild-type (WT) LOVhk, NepR, and PhyR. Cells were imaged for 7 minutes, as it was expected to be sufficient time to see translocation from the cellular cytosol to the nucleus.

As expected, NepR was observed in the nucleus and images looked similar to images of the nuclear dye, which confirms that the NLS worked efficiently (Fig. 3). LOVhk was observed across the whole cell, meaning the sensor was in both the cytosol and the nucleus.

We quantified our automated imaging experiments by developing an analysis script using MATLAB. We designed the script to define the nucleus by the signal from the dye, and then defined the cytoplasm of the cell as the ring of a few pixels radially outside of the nucleus. We

measured fluorescent intensities in both regions, and used the ratio of PhyR signal in the nucleus versus the cytoplasm as a measure of PhyR localization.

In control cell lines without the LOVhk construct, PhyR was observed in both the nucleus and the cytoplasm, and was quantified to have a similar signal in both subcellular compartments. Our quantitative analysis found this localization to be constant across the time course of imaging, including both before and after stimulation (Fig. 4). However, in cell lines with all three constructs, PhyR localization increased its concentration within the nucleus, but not to the same extent observed with NepR (Fig. 3,4). Despite a shift in basal TCS activity prior to stimulation, the responsiveness of the LOV pathway demonstrated no apparent change over the course of the experiment (Fig. 5). Thus, PhyR localization was consistent with LOVhk being active, but in a stimulus-independent manner.

Two mutant histidine kinases, L35T and deltaLOV, retain phosphorylation capabilities but are insufficient to turn-off TCS

We hypothesized that the unexpectedly low responsiveness of LOVhk could be attributed to slow switch-off kinetics. Previous studies have shown that the LOV domain with leucine at a site analogous to Leu-35 in the *B. abortus* LOVhk exhibits some of the slowest switch-off kinetic rates among LOV domains in a different bacteria (17). Kawano *et al.* systematically screened for mutations affecting the switch-off kinetics of the *Avena sativa* LOV domain (17). This study identified the 416T mutation, which resulted in a fast-cycling variant of the *A. sativa* LOV domain (17). A threonine at position 416 results in a switch-off rate 20 times faster than the wild-type *A. sativa* LOV domain (17). The *B. abortus* LOVhk has a leucine at the analogous position in its LOV domain, and was shown to be 100 times slower than the wild-type *A. sativa*

turnover kinetics (17). Thus, we constructed an L35T mutant of the *B. abortus* LOV domain (Fig. 2c).

For comparison, we developed an unregulated histidine kinase construct, referred to as deltaLOV by deleting the entire LOV domain (residues 8-109) from the *B. abortus* construct (Fig. 2b). A previous study demonstrated that deletion of this domain resulted in a constitutively active kinase (18). Consequently, this modification maintains the sensor in a perpetually active phosphorylation state. The deltaLOV construct thus serves as a benchmark for the maximal, unregulated output of p-PhyR.

The incorporation of the faster-cycling LOV domain proved insufficient to restore responsiveness to the LOV pathway in mammalian cells. Cells expressing the L35T construct exhibited no significant change in the PhyR nucleus-to-cytoplasm localization ratio before versus after stimulation (Fig. 5, 6b), demonstrating that the L35T HK construct retained its ability to phosphorylate PhyR. Similarly, cells that carried the deltaLOV construct showed no change in the nucleus-to-cytoplasm localization ratio before versus after stimulation (Fig. 5, 6b).

However, cells expressing either the L35T or deltaLOV constructs exhibited an increase in the basal PhyR nucleus-to-cytoplasm localization ratio compared to control cells lacking a kinase construct (Fig. 4, 6a). This observation suggests that both mutant kinase constructs possess basal activity, therefore, retaining the ability to phosphorylate PhyR. As expected, the deltaLOV construct demonstrated the largest shift in basal activity, exceeding that of the L35T construct.

LovR lowers basal system activity but is insufficient to restore responsiveness to light

Our preliminary data indicated that the LOV pathway required further tuning to restore its light sensitivity. After confirming the ability of the LOVhk mutants to phosphorylate PhyR, and with prior studies having indicated that LovR can function as a phosphatase sink (23), we transiently transfected LovR into cells. This approach tested if competition between LovR and PhyR would be sufficient to restore light responsiveness to the LOV TCS. Cells transiently transfected with the LovR construct did not exhibit a visually different phenotype compared to non-transfected cells (Fig. 7). However as anticipated, we did observe a decrease in the basal level of activity in our LOV pathway (Fig. 8). However, there was no change in pathway activity over time in response to light stimulation (Fig. 8). These results indicate that LovR does negatively regulate PhyR phosphorylation in mammalian cells, but this is not sufficient to restore light sensitivity to the pathway.

H288Q-delLOV-delPAS (LovQ) lowers basal system activity but is insufficient to restore responsiveness to light

Prior in vivo studies showed that an HK with a histidine-to-glutamine (H to Q) mutation resulted in a complete lack of autophosphorylation functionality (21). Sensor histidine kinases usually have multiple signaling domains that control allosteric regulation between two states (20). Either histidine kinases will be in an active state with autophosphorylation and phosphotransferase activities, or in an inactive state with phosphatase activity (20). The *B. abortus* LOVhk has both a LOV domain that is responsive to blue-light, and a PAS (Per-Arnt-Sin) domain that is responsive to oxidative stress (18). Thus, to test a constitutively inactive protein with phosphatase activity for p-PhyR, we deleted both LOV and PAS domains

from the *B. abortus* sensor, and introduced a point mutation, H288Q, generating H288Q-delLOV-delPAS (Fig. 2d). For brevity, the H288Q-delLOV-delPAS construct will be referred to as LovQ.

Cells transiently transfected with the LovQ construct did not exhibit a visually different phenotype compared to non-transfected cells (Fig. 9). In contrast to LovR, results of the introduction of LovQ were inconsistent in terms of the effect on the basal PhyR localization in the presence of the L35T sensor construct (Fig. 10a-c). Thus, the impact of LovQ on pathway activity with the L35T sensor remains inconclusive. However, the presence of LovQ is correlated with a lower basal system activity in the presence of the deltaLOV sensor construct (Fig. 10). Even so, LovQ was insufficient to restore light sensitivity to the LOV TCS with either sensor construct (Fig.10j-l).

2.4 Discussion

In conclusion, the LOV TCS pathway is constitutively active independent of light stimulation across a seven minute timeframe. The results of these experiments are consistent with prior findings demonstrating that TCS HKs retain their ability to phosphorylate their cognate RRs in mammalian cells despite transplantation from distinct domains of life. We tested that finding with a variety of *B. abortus* LOVhk constructs including the wild-type HK as well as two mutant versions. We used an HK missing the LOV domain, previously shown to always be in the active state with autophosphorylation and phosphotransferase activities. As expected, this construct demonstrated the highest amount of TCS activity in its basal state, and it was insensitive to light. Additionally, the L35T mutant HK, with an estimated switch-off rate about 2000 times faster than the wild-type version, similarly did not restore light-sensitivity.

We chose to work with the LOV TCS because it uses a HK that localizes in the cytosol, its light input can be controlled, and we have the ability to quantify the change in localization of the RR. However, perhaps due to the additional PAS domain on the *B. abortus* HK, our constructs did not have the expected light sensitivity. Thus, we tested if adding another component to increase phosphatase activity would restore sensitivity by broadening the dynamic range of p-PhyR in the system. However, those constructs proved to be insufficient as well to restore light stimulation.

While L35T was able to modify the basal TCS activity level, it is undetermined if the results are due to the faster turnover of LOV or to the presence of the PAS domain. Thus, the next step would be to remove the PAS domain from L35T. Alternatively, a construct utilizing the LOV domain, from the *A. sativa* LOVhk could prove to be easier to work with, as it is the more commonly used domain for other biosensors, including the iLID construct which has been successfully used and altered in the Collins Lab.

Notably, we found that LovR reduced the pathway output for cell lines expressing the L35T and deltaLOV HKs. These results support the hypothesis that LovR is a phosphate sink in its native organism. However, to determine this behavior conclusively would require further studies. In particular, our studies demonstrated that researchers seeking to characterize the functionality of components in the LOV pathway, and by extension other TCS as well, could benefit from utilizing mammalian cells by allowing the components to interact with one another without purification while eliminating crosstalk with other pathways in the native cells. Albeit, there is room for improvement by controlling expression levels, and that itself could be helpful for researchers testing out different concentration levels for each component.

LovQ was shown to consistently lower basal TCS activity levels with deltaLOV, but not with L35T, which may be due to the low number of cells counted in the final quantification. Thus, future research should test more cells with the L35T construct to further support the current findings that LovQ does influence basal activity. Currently it is inconclusive whether LovQ lowers basal activity; however, it is likely that LovQ would lower basal activity based on our results with the deltaLOV construct.

These sets of experiments would benefit from confocal imaging to better distinguish between subcellular compartments (i.e. the nucleus and the cytoplasm), and could potentially identify subtle shifts over time if the overlapping cytoplasm and nucleus in the epifluorescent images were sufficient to dampen changes in localization.

2.5 Materials and Methods

Design and molecular generation of DNA constructs

NCBI Reference Sequence: WP_002969337.1 was used as the wild-type *B. abortus*. Each LOVhk variant is tagged with mTurquoise2 at the C-terminus following an EFGGGGS linker in which the first two amino acids correspond to an EcoRI restriction site. NepR is tagged with iRFP670 at the C-terminus following a GGGGS linker with a unique MluI restriction site in between, translating into TR, and with two copies of the SV40 NLS downstream of the fluorescent tag. PhyR is tagged with mScarlet at the C-terminus following a GGGGS linker. Each TCS plasmid is under the regulation of a EF1a promoter, codon optimized for expression in *Homo sapiens* cells, and in a pLenti 2nd generation vector backbone carrying an ampicillin bacterial resistance marker, which was double restriction enzyme digested to allow insertion of the TCS component. Each wild-type TCS component was synthesized with human codon

optimization by Twist Biosciences, including: LOVhk, NepR, and PhyR. Each fluorescent tag was amplified by PCR along with the linkers fusing them to the TCS component of interest. Then each plasmid was constructed in its own Gibson Assembly procedure, followed by transformation of Stbl3 *E. coli* cells, which were plated on agar plates for selection under carbenicillin, as a more stable alternative to ampicillin. For both mutant versions of LOVhk, the WT construct was double restriction digested after the Kozak sequence and before the linker to allow for the insertion of the mutated version. Each plasmid sequence was confirmed by whole plasmid sequencing services by Plasmidsaurus (SNPsaurus).

deltaLOV was developed by deleting residues analogous to the homolog in *A. sativa* 8-109 (18). Amplified by PCR, we generated two fragments for later synthesis, deltaLOVa and deltaLOVb. deltaLOVa retained the 3' end of the EF1a promoter through Pro-33 of the WT *B. abortus* LOV domain. deltaLOVb retained Val-135 of the WT *B. abortus* LOV domain through a short segment of the N-terminus of mTurquoise. Gibson primers were designed to join deltaLOVa and deltaLOVb together resulting in deltaLOV construction, which encodes a total of 388 amino acids, through a multi-fragment Gibson assembly reaction.

The L35T LOVhk was created by introducing a point mutation at the Leu-35 of WT LOVhk from *B. abortus*, which is analogous to position 416 from AsLOV2 as used in prior studies (17). We amplified LOVhk in two fragments, L35Ta and L35Tb, and used the Gibson primers to replace two nucleotides that result in a single amino acid change. Gibson primers were designed to assemble L35Ta and L35Tb together to result in the construction of a L35T mutant through a multi-fragment Gibson assembly reaction.

LovR was synthesized by Twist Biosciences into a pTwist EF1 Alpha backbone. The LovR insert was designed from the N to C termini as follows: LovR, small GSS linker, tPT2A sequence (similarly used in Chapter 3), and mCitrine tagged by an NLS.

H288Q-delLOV-delPAS, also referred to as LovQ, was created via a multi-fragment Gibson assembly reaction similar to that used in the construction of L35T and deltaLOV. The LovR plasmid was double restriction digested to remove the LovR domain to create an expression backbone. The LovQ domain was amplified and inserted at the 5' end of the tPT2A sequence.

Cell culturing

HEK293 cell lines were maintained at 37 °C, 5% CO2 in DMEM medium, supplemented with 9% (vol/vol) FBS. Passaging occurred at 70–80% confluency roughly every 2-3 days in six-well plates.

Generation of transient and stable HEK293 cell lines with LOV TCS

For development of stable cell-lines, we used 2nd generation lentiviral-mediated gene transfer. HEK-293T cells were transfected in OPTI-MEM using PEI as the transfection reagent. Media was changed to DMEM containing 9% FBS after 16 hours. Supernatant was collected at 24 hours post media change and filtered. Then, HEK293T cells were infected with lentivirus containing supernatant in a 1:10 polybrene solution of DMEM supplemented with 9% FBS. Finally, cells were selected via antibiotic selection per gene integration.

96-well culture plates were used in transfection experiments. Wells were seeded with 1.0×10^5 cells per mL and 100uL per well 16-24 hours before transfection. The experimental cell

line has all three main components stably expressed, and the control line is missing integration of any LOVhk encoding plasmids.

For transfection, a total of 100ng of DNA was resuspended in OPTI-MEM without serum in combination with PEI in a 1:30 ratio of PEI to OPTI-MEM ratio plus the volume for DNA. The cells were incubated for 16-24 hours before imaging.

Microscopy and imaging protocols for experimental procedures

All imaging was performed on a Nikon Ti microscope using epifluorescence illumination. Images were acquired using a Nikon Plan Apo 20X objective (NA 0.75) and Zyla 4.2 scientific CMOS cameras, with appropriate filter sets for each fluorescence channel.

To test the responsiveness of the LOV pathway in mammalian cells, cells were kept in the dark before the experiment and plated in a 96-well plate. The media used for the imaging experiments was replaced with a low-fluorescence L15 medium. Plates were placed on a microscope in the dark, and imaged across 7 minutes. Every thirty seconds cells were imaged across the three fluorescent channels as well as UV for a nuclear stain to be able to count cells in any frame and calculate where the nuclei are for downstream analysis. Then, after the 7 minute interval, brightfield images were taken of the cells to capture and evaluate the health condition of the cells by the end of the experiment.

Images were uniformly processed with custom MATLAB software. We used image registration to align images taken on the two cameras. Cell nuclei were identified and segmented using image sharpening to enhance edges, followed by thresholding and object detection using MATLAB's "regionprops" function. We recorded the coordinates for each nucleus and a corresponding ring, of two pixels, beginning just outside the nuclear boundary as the cytosol for

that cell. We tracked the movements of each cell from frame to frame over the course of the experiment to adjust for random cell motility. We computed a series of values per cell region (i.e., nucleus or cytosol) of fluorescent signal before and after stimulation, where the first frame is considered before, and every subsequent frame is considered to be after stimulation. We used the median value signal per subcellular region to calculate the ratio of PhyR in the nucleus to cytosol. Finally, we plotted the frequency distributions of the ratios calculated to make the figures referenced in this chapter.

2.6 Acknowledgments

Many thanks to AT for her help during this project, credit for assembling the WT LOVhk, deltaLOV, L35T, NepR-NLS, Response Elements, and HnoC-VPR plasmid constructs. Nothing but gratitude for AC as she was essential to the team in developing the LOV TCS and support. SS was critical to helping establish microscopy experiments to test TCS in the Collins Lab. Thanks also to KBN for his support throughout our tenure in the lab, pushing me as a scientist and helping troubleshoot microscopy and analysis. Many thanks to Dr. Collins and the whole Collins lab for their support in completing this project.

2.7 Figures

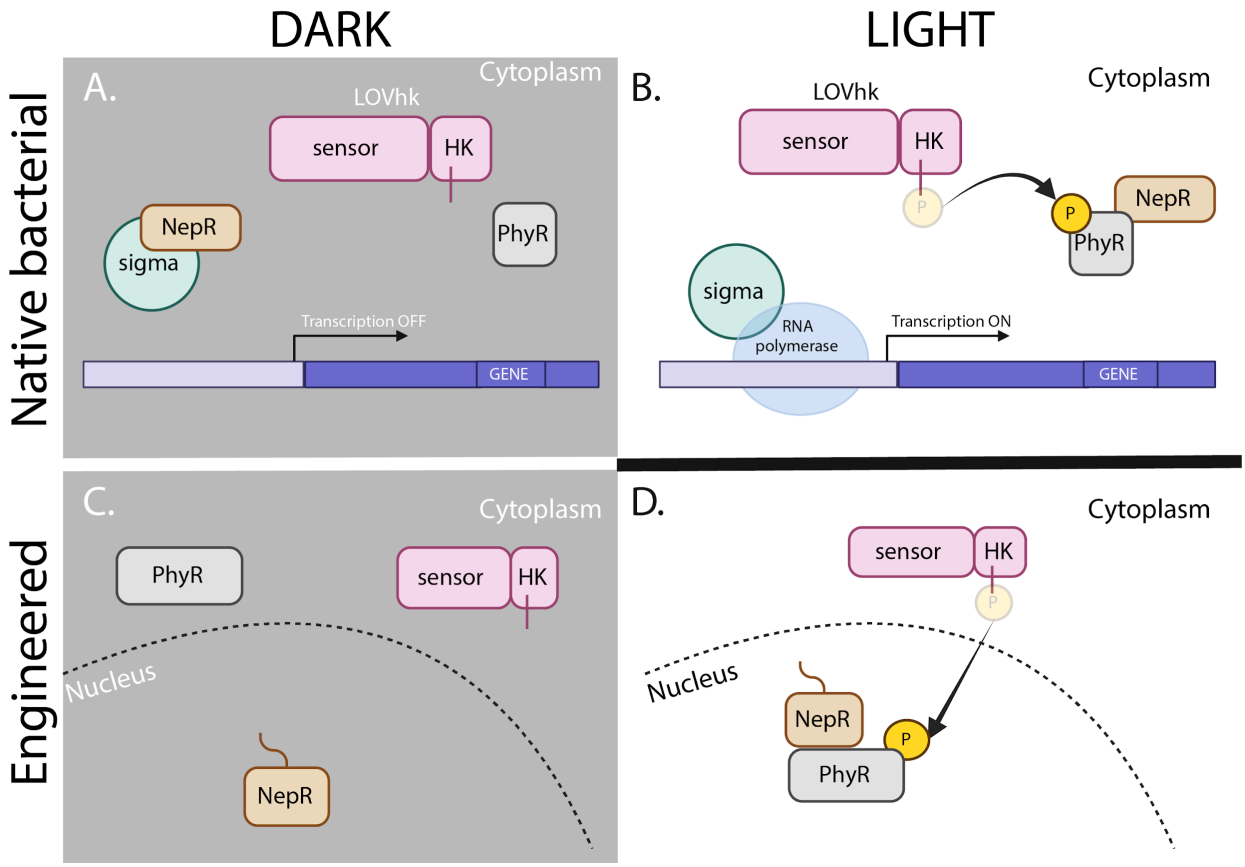

Figure 1. LOV TCS overview. (A) An illustration of the *B. abortus* LOV pathway before light stimulation. (B) LOV pathway after light stimulation activates LOVhk autophosphorylation, followed by a phosphotransfer, which results in transcriptional regulation through NepR and a sigma factor in the bacteria. (C) Depicts the engineered LOV TCS in the dark in mammalian cells with a nucleus. NepR is localized in the nucleus due to a nuclear localization sequence. (D) Hypothesized response from light-stimulation initiating activation of the pathway.

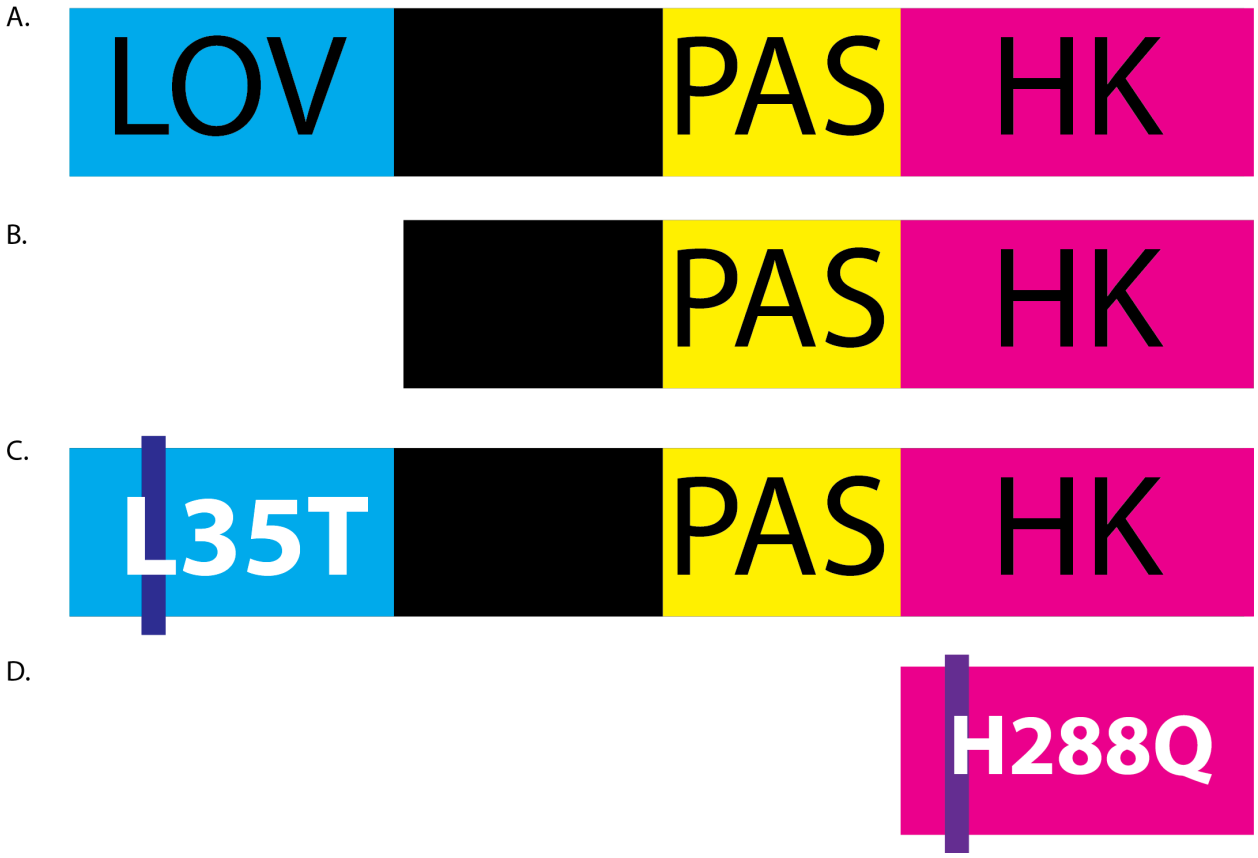

Figure 2. Schematic representation of LOVhk constructs. A representation of (A) WT LOVhk next to the three mutated versions of the protein, aligning the domains for comparison. (B) deltaLOV, which has the whole LOV domain deleted. (C) L35T, showing the leucine-to-threonine (L to T) substitution at Leu-35 in the *B. abortus* LOVhk for the design of the fast-cycling LOV domain. Finally, (D) H288Q-delLOV-delPAS (LovQ) represents the deletion of both the LOV and PAS domains with the histidine-to-glutamine (H to Q) substitution.

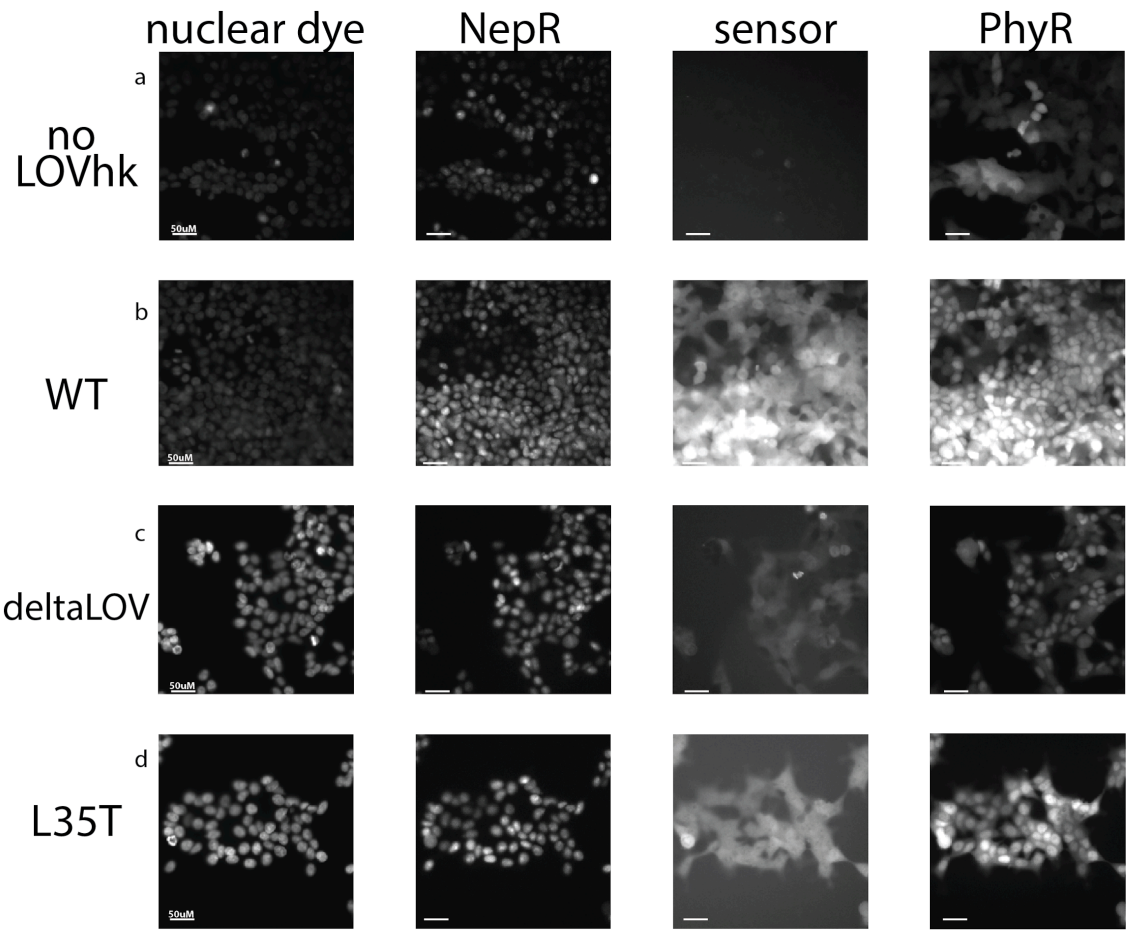

Figure 3. A histidine kinase is sufficient for relocalization of PhyR into the nucleus.

HEK293 cells at t=0, with all genes genomically integrated to express a version of a LOV TCS. Columns demonstrate the signal from different channels imaged simultaneously. All cells were stably expressing PhyR-mScarlet and NepR-iRFP. Rows are cells with different versions of a LOVhk sensor: (A) no LOVhk sensor, (B) wild-type LOVhk, (C) LOV domain deleted, and (D) with fast-cycling LOV with the point mutation L35T. Cell images from one day, representative of replicates conducted over three independent days. 50 μM scale bar.

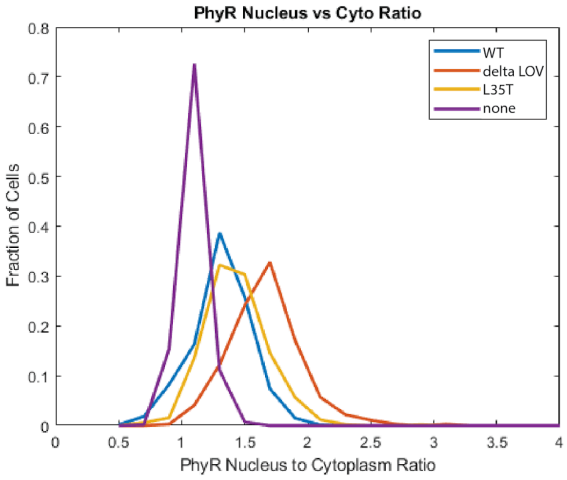

A.
Basal Nuc vs. Cyto Ratio for WT = 1.312 (2371 cells)
Basal Nuc vs. Cyto Ratio for deltaLOV = 1.658 (369 cells)
Basal Nuc vs. Cyto Ratio for L35T = 1.430 (515 cells)
Basal Nuc vs. Cyto Ratio for none = 1.090 (3188 cells)

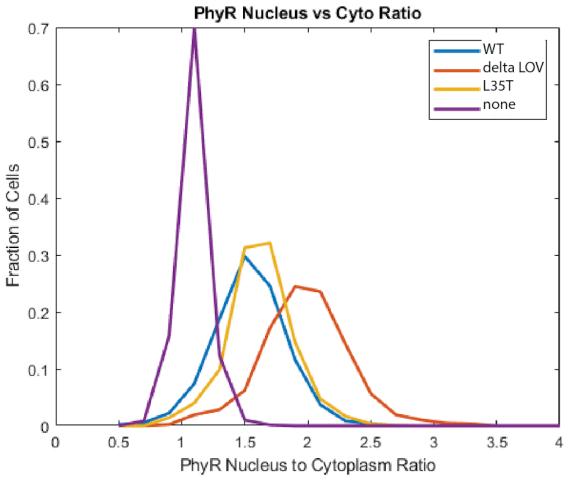

B.
Basal Nuc vs. Cyto Ratio for WT = 1.539 (1814 cells)
Basal Nuc vs. Cyto Ratio for deltaLOV = 1.980 (887 cells)
Basal Nuc vs. Cyto Ratio for L35T = 1.622 (1209 cells)
Basal Nuc vs. Cyto Ratio for none = 1.090 (710 cells)

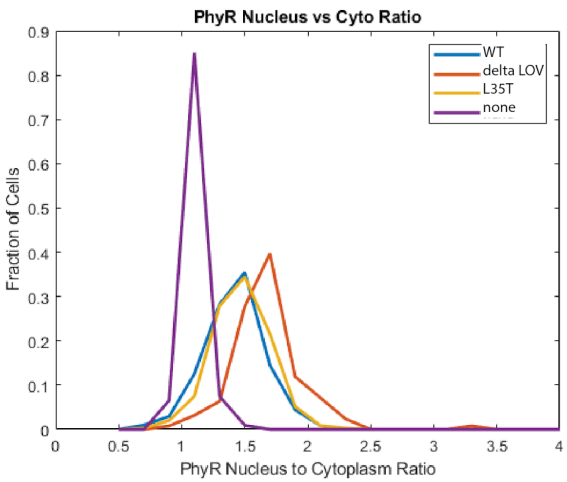

C.
Basal Nuc vs. Cyto Ratio for WT = 1.418 (814 cells)
Basal Nuc vs. Cyto Ratio for deltaLOV = 1.677 (126 cells)
Basal Nuc vs. Cyto Ratio for L35T = 1.470 (348 cells)
Basal Nuc vs. Cyto Ratio for none = 1.099 (107 cells)

Figure 4. Baseline activity of LOVhk constructs before light stimulation. The upper panels show the ratio of PhyR detected in the cell nucleus over the amount in the cytoplasm at t=0,

when cells were kept in the dark prior to experiments. Each subpanel represents the results from a different day. Across the three days, ‘none’ annotates cells with no sensor component expressed, ‘deltaLOV’ provides cells with a sensor mutated into an always-on state with peaks on the far right, ‘WT’ indicates the wild-type LOV sensor, and ‘L35T’ is a mutated version of LOV hypothesized to have a turnover rate about 2000x faster than WT.

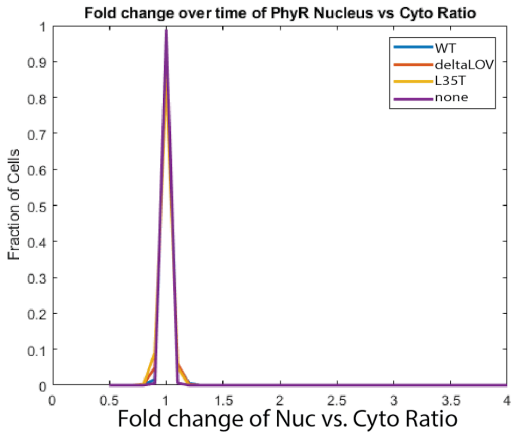

A.
Fold change of Nuc vs. Cyto Ratio for WT = 1.005 (2371 cells)
Fold change of Nuc vs. Cyto Ratio for deltaLOV = 1.002 (369 cells)
Fold change of Nuc vs. Cyto Ratio for L35T = 0.997 (515 cells)
Fold change of Nuc vs. Cyto Ratio for none = 0.999 (3188 cells)

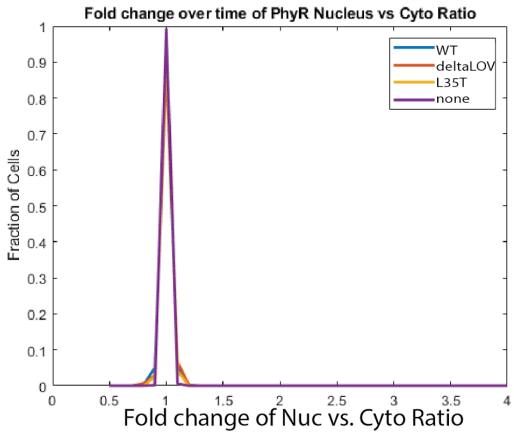

B.
Fold change of Nuc vs. Cyto Ratio for WT = 1.000 (1814 cells)
Fold change of Nuc vs. Cyto Ratio for deltaLOV = 1.003 (887 cells)
Fold change of Nuc vs. Cyto Ratio for L35T = 1.002 (1209 cells)
Fold change of Nuc vs. Cyto Ratio for none = 1.000 (710 cells)

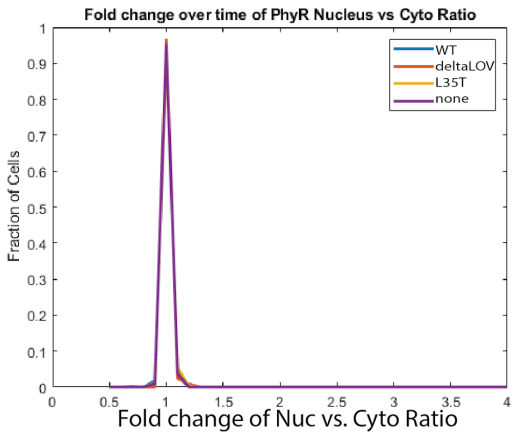

C.
Fold change of Nuc vs. Cyto Ratio for WT = 1.003 (814 cells)
Fold change of Nuc vs. Cyto Ratio for deltaLOV = 1.009 (126 cells)
Fold change of Nuc vs. Cyto Ratio for L35T = 1.004 (348 cells)
Fold change of Nuc vs. Cyto Ratio for none = 1.003 (107 cells)

Figure 5. LOVhk protein activity remains unchanged by light stimulation over time. The upper panels show the recorded fold change of the ratio of PhyR detected in the cell nucleus over the amount in the cytoplasm by the end of the experiment, 7 minutes. Each subpanel represents the results from a different day. Across three days the results were identical, indicating that there is no response to light stimulation over the course of the experiment. 'none' indicates cells with

no sensor, ‘deltaLOV’ indicates cells with a sensor mutated into an always-on state, ‘WT’ indicates the wild-type LOV sensor, and ‘L35T’ is a mutated version of LOV hypothesized to have about a 2000x faster turnover rate.

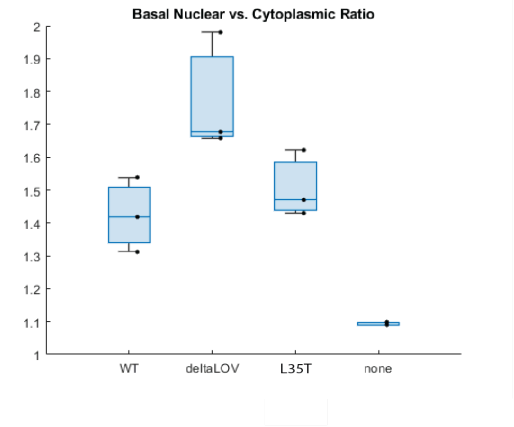

A.
Cumulative medians per day of the basal ratio between PhyR in the nucleus over the cytoplasm, per sensor type.

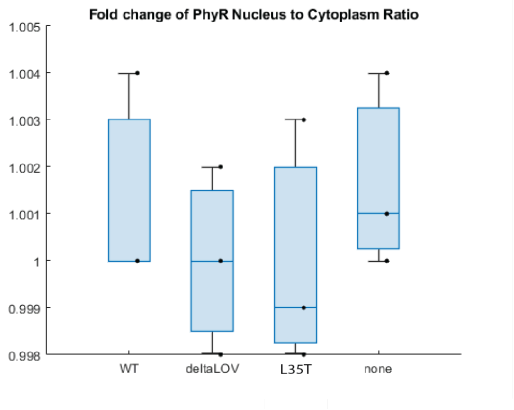

B.
Cumulative medians per day of the fold change over time of the ratio between PhyR in the nucleus over the cytoplasm, per sensor type.

Figure 6. Cumulative data of WT LOV TCS. (A) A boxplot shows the range of the medians per day of basal activity, based on the PhyR nucleus versus cytoplasm ratio at t=0. (B) A boxplot shows the range of the medians of the recorded responsiveness of the system, by measuring the fold-change in the ratios at the start versus the end of the time course. Three independent biological replicates were performed for each condition.

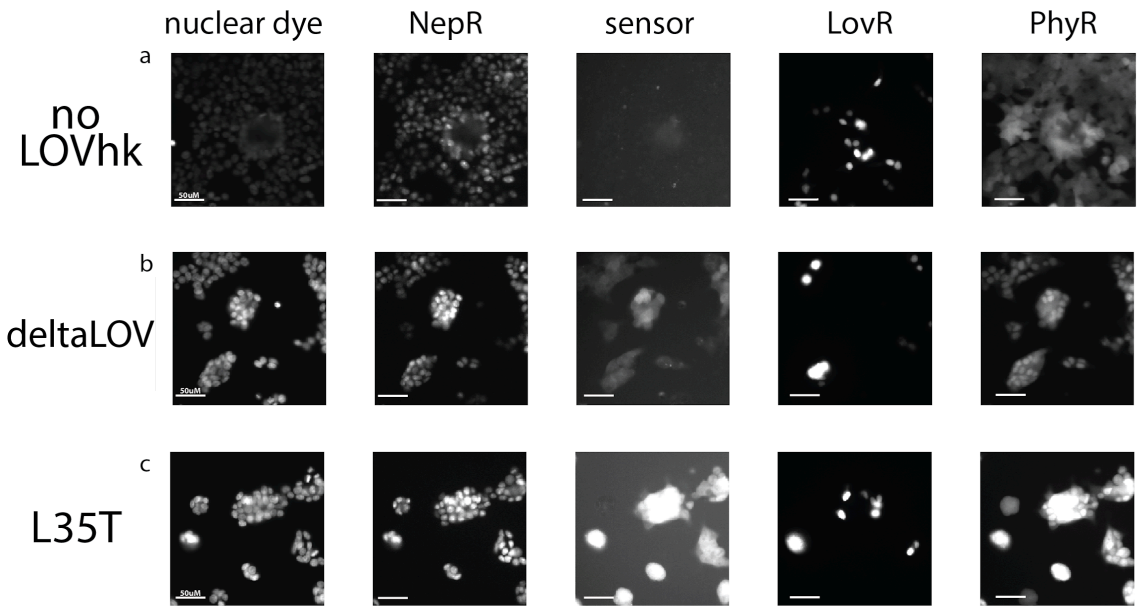

Figure 7. LovR is insufficient to restore TCS sensitivity to light. HEK293 cells with PhyR-mScarlet-I, NepR-iRFP670, and the indicated LOVhk construct genomically integrated were transiently transfected with LovR. Images are shown for t=0, before light stimulation. Columns demonstrate the signal from different channels. Rows are cells with different versions of a LOVhk sensor: (A) no LOVhk sensor, (B) LOV domain deleted, and (C) with fast-cycling LOV from the point mutation L35T. Cell images from one day, representative of replicates conducted over three independent days. 50 μM scale bar.

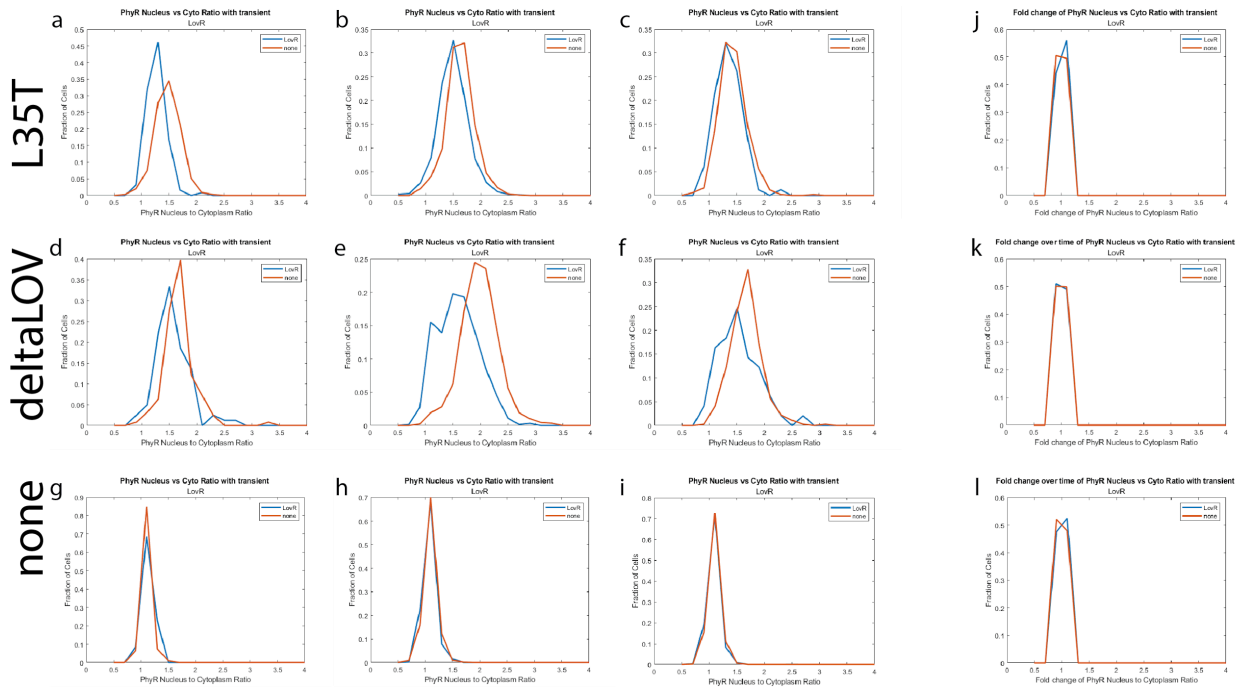

Figure 8. LovR shifts basal activity but is not sufficient to restore light responsiveness of the LOV TCS pathway. Labels on the left indicate the stable genomically integrated sensors for the corresponding row of data plots; 'L35T' is a mutated version of LOVhk that is hypothesized to turn over faster than the WT, 'deltaLOV' is a mutated LOV that is known to be always activated, and 'none' means no stably integrated sensor was present. The series of panels (a-i) compares the basal ratio of PhyR in the nucleus over that observed in the cytoplasm at t=0 for LovR positive cells in samples transfected with LovR (blue lines) or negative 'none' cells in samples that were not transfected with LovR (orange lines). Each column shows the results from a different day. The three panels on the right (j-l) show the fold change in the PhyR nucleus-to-cytoplasm ratio after light stimulation, comparing the same LovR positive (blue) versus negative (orange) cells. These are only from one day, but they are representative of the results from all three days. Number of cells (n) for each subpanel were (LovR+/LovR-): a 126/348, b 759/1209, c 84/515, d 81/126, e 788/887, f 49/369, g 35/107, h 959/710, i 1673/3188, j 84/515, k 49/369, l 1673/3188.

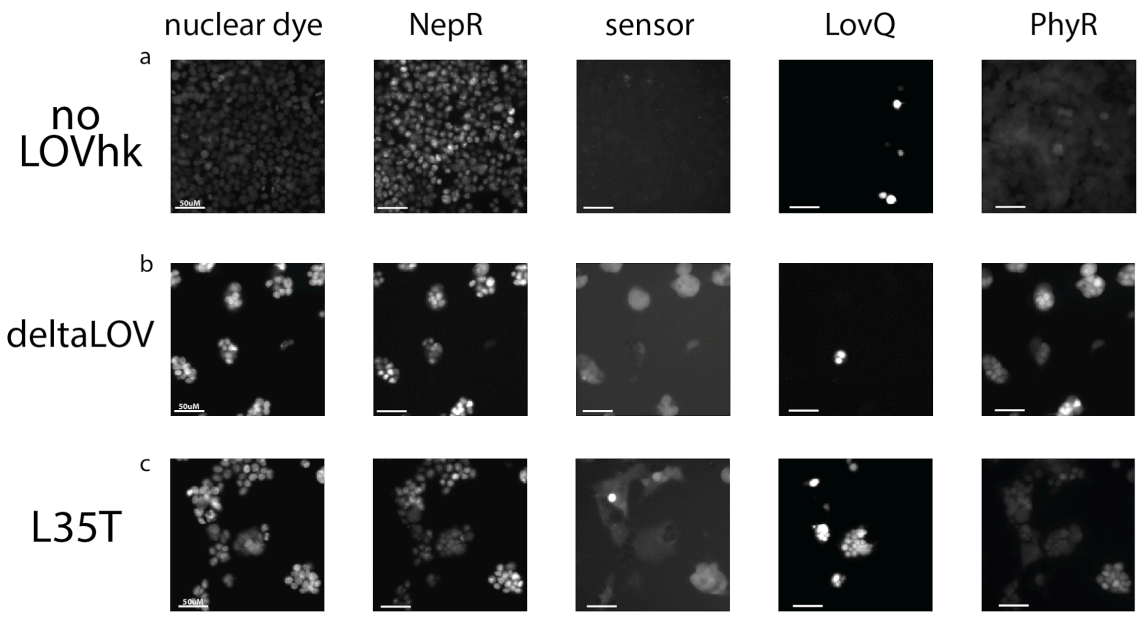

Figure 9. H288Q-delLOV-delPAS (LovQ) is insufficient to restore TCS sensitivity to light. HEK293 cells with PhyR-mScarlet, NepR-iRFP, and the indicated LOVhk construct genomically integrated were transiently transfected with LovQ. Columns demonstrate the signal from different channels, imaged at t=0. Rows are cells with different versions of a LOVhk sensor: (A) no LOVhk sensor, (B) LOV domain deleted, and (C) with fast-cycling LOV from the point mutation L35T. Cell images from one day, representative of replicates conducted over three independent days. 50μM scale bar.

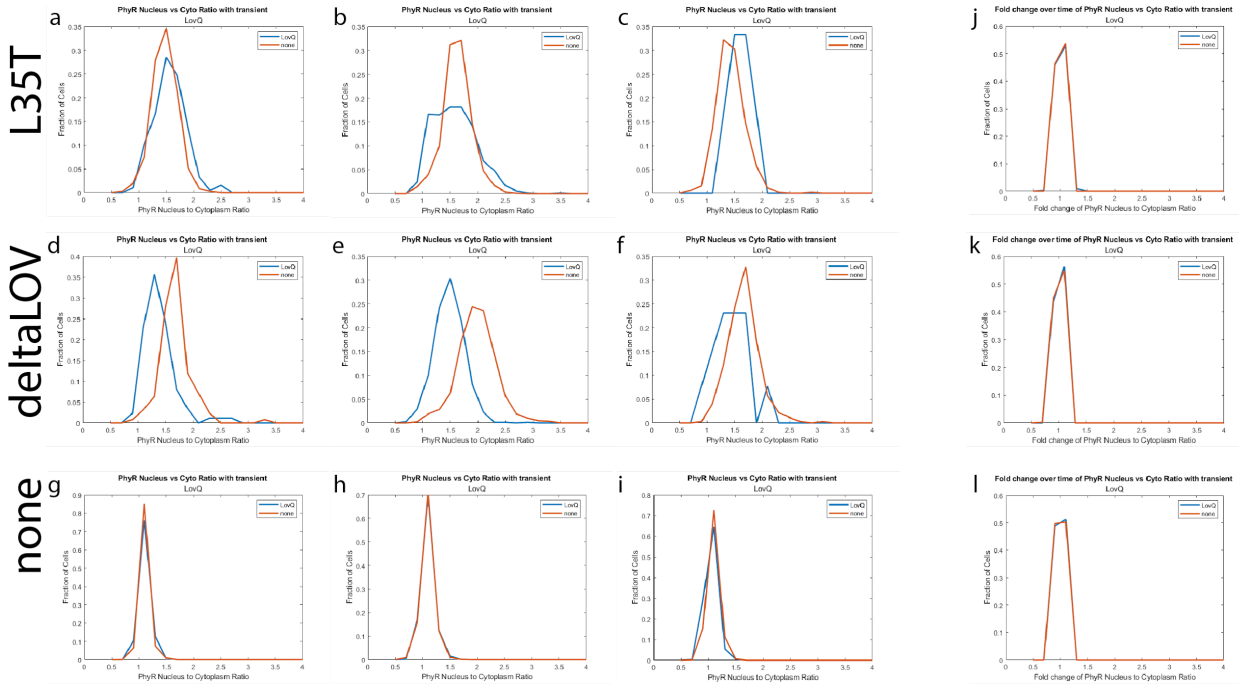

Figure 10. LOV H288Q-delLOV-delPAS shifts basal activity but is not sufficient to restore the light responsiveness of the LOV TCS pathway. Lov H288Q-delLOV-delPAS (LovQ) is a mutant construct from wild-type LOVhk, where both LOV and PAS domains were deleted and the H288Q amino acid mutation was introduced. Labels on the left indicate the stably genomically integrated sensors for the corresponding row of data plots; 'L35T' is a mutated version of LOV that is hypothesized to turn over faster than the WT, 'deltaLOV' is a mutated LOV that is known to be always activated, and 'none' means no stably integrated sensor. The series of panels (a-i) compares the basal ratio of PhyR in the nucleus over that observed in the cytoplasm at t=0, and the curves represent cells that are LovQ positive 'LovQ' (blue lines) or negative 'none' (orange lines). Each column shows the results from a different day. The three panels on the right (j-l) show the fold change in the PhyR nucleus-to-cytoplasm ratio after light stimulation, comparing the same LovQ positive (blue) versus negative (orange) cells. These representative results from one day showed no change, and are representative of the results from

all three days. While we saw shifts in the basal state of the TCS pathway, there was no observed change in the localization of PhyR in response to the stimulation with blue light over the 7 minute time course. Number of cells (n) for each subpanel were (LovQ+/LovQ-): a 214/348, b 734/1209, c 6/515, d 98/126, e 788/887, f 13/369, g 238/107, h 857/710, i 1987/3188, j 734/1209, k 788/887, l 857/710.

Chapter 3

Unresolved questions: Ambiguous results from transient Hno TCS transfections in mammalian cells

Diana Sernas, Sabrina Truoung, Aditi Thambala, Alex Calderon, Sarah Sun, Shashank Shastry, Sean R. Collins

Department of Microbiology and Molecular Genetics, University of California, Davis, Davis, CA, USA.

3.1 Preface

This chapter describes how we tested and characterized the Hno TCS pathway from *Shewanella oneidensis* in HEK293 cells. Section 3.2 provides our rationale for choosing Hno for proof-of-principle experimentation, a review of how the components in the TCS behave in their native environments, and an overview of how the Hno TCS was adapted for integration and testing in human cells. In section 3.3, there is a summary of our preliminary data from the engineered Hno pathway in mammalian cells. Section 3.4 provides an interpretation of the results thus far, technical difficulties faced, and suggestions for overcoming them in future work. Section 3.5 provides a brief summary of the design and molecular cloning of each of the components used, and transfection of cells for experiments. Lastly, section 3.6 is the accumulated figures referenced to throughout Chapter 3.

3.2 Introduction

Hno pathway as a model cytoplasmic TCS for cell engineering

We selected the Hno pathway, from *Shewanella oneidensis* (24), as a model TCS pathway for use in mammalian cells because it utilizes a cytoplasmic sensing kinase, and is sensitive to nitric oxide which we can monitor and control as a soluble signal for experiments. We expanded the landscape to test TCS that utilize cytoplasmic sensors, as we hypothesized that cytoplasmic sensors could overcome the prior challenges with improper subcellular localization and activity of transmembrane sensors. Additionally, this TCS results in the more common output of transcriptional regulation, a much more well characterized response for these types of pathways (10). Transcriptional outputs for TCS are highly adaptable as scientists can utilize them to regulate any gene of interest. Specifically, we could adapt the Hno circuit for mammalian cells such that pathway activation results in suppression of the expression of the reporter gene; similar strategies have been used in screens to identify positive results for synthetic proteins in prior studies (25). Reporter gene expression is easily measured, which makes it ideal for proof-of-principle engineering applications to study candidate TCS of interest in living human cells. Furthermore, the capability of HnoC to oligomerize offers promising opportunities for cell engineering applications. This property could be harnessed in the development of biosensors, such as FRET-based systems, an area in which the Collins Lab has extensive expertise. Additionally, it may provide insights into other signaling networks governed by oligomerization processes native or foreign to mammalian cells.

Hno in bacteria

Nitric oxide (NO) is a signaling molecule detected across all domains of life, and specifically plays a role in regulating bacterial biofilm formation in mammalian hosts (24,26). This includes the bacteria associated with cystic fibrosis (26). Bacterial biofilms are protective for a variety of bacteria as they switch between mobile and immobile lifestyles(24,26). Biofilm formation by some bacterial species is regulated by NO sensing pathways involving heme-nitric oxide/oxygen (Hno) binding domains (24,26).

In *S. oneidensis*, the Hno signaling network relies on the histidine kinase HnoK, which can autophosphorylate and transfer a phosphate group to downstream response regulators (24). HnoK phosphorylation is dependent on its regulating protein, HnoX; when HnoX is NO-bound, HnoX blocks HnoK phosphorylation (24) (Fig. 1). The presence of HnoX distinguishes this pathway from most TCS pathways. Typically, ligands bind directly to a TCS sensor HK for activation (10), but in this case, NO-bound HnoX inhibits HnoK autophosphorylation (24). Once phosphorylated, p-HnoK can transfer the phosphate group to HnoC or other RRs (25). p-HnoK, can transfer a phosphate group to HnoB, which leads to an increase in hydrolysis of cyclic-di-GMP, or HnoK can phosphorylate HnoD, which acts as an allosteric effector fine-tuning HnoB activity (24). In contrast to the other RRs downstream of HnoK, HnoC contains a DNA binding effector domain and it regulates the expression of all components of the *S. oneidensis* Hno network (24).

Prior studies have shown that the capability of HnoC to regulate transcription is linked to its tetrameter formation (24). HnoC forms a tetramer when unphosphorylated and binds to DNA (24). HnoC tetramers are hypothesized to dissociate into monomers when the protein is

phosphorylated (24). Phosphorylation disrupts the tetramer, leading to dissociation from DNA and relief of transcriptional repression (Fig. 1). These properties make HnoC an ideal candidate as a component for testing TCS integration into mammalian cells.

Hno adapted for mammalian cells

To adapt the *S. oneidensis* TCS for use in mammalian cells, we modified the Hno sensor components. Specifically, we inserted a tPT2A sequence between HnoX and HnoK. This modification allowed for the expression of both proteins from a single plasmid, thereby reducing the number of plasmids required for transfection into HEK293 cells. The tPT2A sequence has been shown to cause the ribosome to release the nascent polypeptide and resume translation, resulting in robust expression of both proteins flanking the tPT2A sequence as separate polypeptides (27). However, the protein at the C-terminus of the tPT2A sequence, in this case HnoK, is expressed at a lower level than the protein at the N-terminus, HnoX. Since HnoX acts as a suppressor of HnoK, we developed a plasmid construct consisting of only HnoK that we hypothesized would be constitutively active. Both versions of the Hno *S. oneidensis* sensor plasmids have a short linker at the N-terminus of HnoK fusing it to an RFP tag for confirmation of expression and subcellular localization.

To enhance the ability of HnoC to regulate transcription, we fused VPR to the C-terminus of HnoC, followed by a CFP tag. To provide the ability for the TCS to regulate transcription, we designed a response element (RE) that was successfully genomically integrated into HEK293 cells. The RE consists of two identical HnoC binding motifs in tandem. The motif was defined in prior studies (24) characterizing the capability of HnoC to bind DNA. Downstream of the HnoC

binding sites are a minimal promoter and TATA box regulating expression of a YFP reporter gene.

3.3 Results

HnoC is sufficient for activation of TCS in mammalian cells

We set out to test and measure the TCS activity using live cell imaging experiments. To verify the expression and localization of each TCS component, we fused them with spectrally distinct fluorescent proteins at their C-termini, ensuring no overlap in excitation ranges. We established a baseline by imaging a stable cell line expressing only the synthesized Response Element (RE). To identify and analyze individual cells, we stained all cells with an ultraviolet (UV) nuclear dye. To assess the responsiveness of the *S. oneidensis* Hno pathway in HEK293 cells, we tested expression of the response regulator (RR) HnoC in combination with either the HnoX-HnoK or HnoK construct alone. We expected that Hno TCS to increase transcription activity for the reporter gene in the presence of nitric oxide (Fig. 1)

As expected, cells without any TCS construct do not express the reporter gene, YFP (Fig. 2a). HnoC was observed to be sufficient for transcription of the reporter gene for the Hno TCS in mammalian cells (Fig. 2). Some cells imaged with only HnoC were capable of YFP expression (Fig. 2b). Thus, in conclusion many cells expressing the HnoC constructs express YFP, but with substantial cell-to-cell heterogeneity.

HnoK vs HnoXK: Is HnoX regulating HnoK in the absence of nitric oxide?

We expected the expression of HnoK would decrease overall TCS activity by increasing phosphorylated-HnoC. Thus far, we have seen no obvious suppressing effect of expressing HnoX

and HnoK on the ability of HnoC-VPR to activate the reporter gene. We saw that cells expressing HnoX, HnoK, and HnoC were still able to activate transcription of the reporter gene (Fig. 2c). Therefore, we sought to test the ability of HnoK to regulate HnoC, free of any suppressive behavior from its native regulator HnoX. Similarly, cells with both HnoK and HnoC were YFP positive (Fig. 2d). In summary, we did not see evidence that the HnoK construct, lacking suppression from HnoX, was able to regulate HnoC.

3.4 Discussion

Due to technical challenges in generating stable cell lines and achieving adequate transient co-transfection efficiency with two separate plasmids, I was unable to obtain a quantitative dataset. From the current data, I hypothesize that the VPR fused to HnoC is sufficient for activating transcription of the reporter gene, even in the context of HnoK kinase activity, thus removing the responsiveness of the pathway to NO.

Our strategy for stimulation of cells was to use a NO donor, such as sodium nitroprusside (28) or spermine NONOate (29). However, due to initial preliminary results, we did not advance to doing careful stimulation experiments with the system. As the system is currently designed, I hypothesize that the expression of YFP should increase with the addition of NO. The apparent output of the pathway even in the absence of NO made this difficult to test. For future efforts to make a TCS that is responsive to NO in mammalian cells, it may be important to use a weaker transcription factor than VPR in combination with human cell lines that have the TCS components stably integrated into the genome. The stable expression of components might provide lower and more consistent expression levels, which might lead to better pathway function. Additionally, an investigation of how much HnoC is able to tetramerize in mammalian

cells could help elucidate whether the sensitivity of the system can be restored by focusing on the sensor constructs, or if modification of the HnoC construct would be necessary.

Another avenue that could be worth further investigation to establish the Hno TCS in mammalian cells is more thorough testing of the HnoK gene. To test if HnoK can turn off the Hno TCS, I suggest using a weaker transcription activation domain such as VP64 and an alternative genome integration method. Furthermore, measuring how much HnoK can cause dissociation of HnoC tetramers could help illuminate the effectiveness of HnoK regulation of HnoC. Additionally, because there was no obvious difference between the HnoXK and HnoK conditions, it would help to know if HnoX and HnoK are able to appropriately associate, despite the remaining amino acids introduced from the tPT2A sequence in between them.

3.5 Materials and Methods

Design and molecular generation of DNA constructs

HnoX is co-expressed upstream of HnoK by a tPT2A sequence. Each HnoK is tagged with mScarlet at the C-terminus following an GGGGS linker. At the C-terminus of HnoC is a TNSGASGSGNA linker with the first two amino acids corresponding to a MluI restriction site, VPR, a Nuclear Export Sequence, another linker with a EFGGGGS sequence, and finally mTurquoise. The response element (RE) genomically integrated into HEK293 cells has two identical tandem HnoC binding sites with no space in between, about 160 bp upstream of a minimal promoter, TATA box, and Kozak sequence at the -1 position to the reporter gene mCitrine. Each TCS plasmid is under the regulation of an EF1a promoter, codon optimized for expression in *Homo sapiens* cells, and in a pLenti 2nd generation vector backbone carrying an ampicillin resistance gene, which was double restriction enzyme digested to allow insertion of

the TCS component. Each TCS component was synthesized with human codon optimization by Twist Biosciences through the GGGGS linker, including: HnoX-tPT2A-HnoK, HnoK, HnoC, and RE. Each fluorescent tag was amplified by PCR. Then each plasmid was constructed in its own Gibson Assembly procedure, followed by transformation of Stbl3 *E. coli* cells, which were plated on agar plates for selection under carbenicillin, as a more stable alternative to ampicillin.

Cell culture, and generation of transient and stable HEK293 cell lines to test the Hno TCS

96-well culture plates were used in transfection experiments. Wells were seeded with 1.0×10^5 cells per mL and 100 uL per well 16-24 hours before transfection. The experimental cell line has the RE stably integrated. All other components were transfected transiently for imaging experiments. The HEK293 cell line was maintained at 37 °C, under 5% CO2 in DMEM medium, supplemented with 9% (vol/vol) FBS. Passaging occurred at 70–80% confluency roughly every 2-3 days in six-well plates.

For development of stable cell-lines, we used 2nd generation lentiviral-mediated gene transfer. HEK-293T cells were transfected in OPTI-MEM using PEI as the transfection reagent. Media was changed to DMEM containing 9% FBS after 16 hours. Supernatant was collected at 24 hours post media change and filtered. Then, HEK293T cells were infected with lentivirus containing supernatant in a 1:10 polybrene solution of DMEM supplemented with 9% FBS. Finally, cells were selected via antibiotic selection per gene integration.

For transfection, 100 ng of DNA total was resuspended in OPTI-MEM without serum in combination with PEI in a 1:30 ratio of PEI to Optimem ratio plus the volume for DNA. The cells were incubated for 16-24 hours before imaging. The media used for the imaging experiments was replaced with a low-fluorescence L15 medium.

Microscopy and imaging protocols for experimental procedures

All imaging was performed on a Nikon Ti microscope using epifluorescence illumination. Images were acquired using Nikon Plan Apo 20X objective (NA 0.75) and Zyla 4.2 scientific CMOS cameras, with appropriate filter sets for each fluorescence channel.

Images were uniformly processed with custom MATLAB software. We used image registration to align images taken on the two cameras. With limited cells that sufficiently expressed multiple transiently transfected components, rigorous computational analysis was not possible.

3.6 Figures

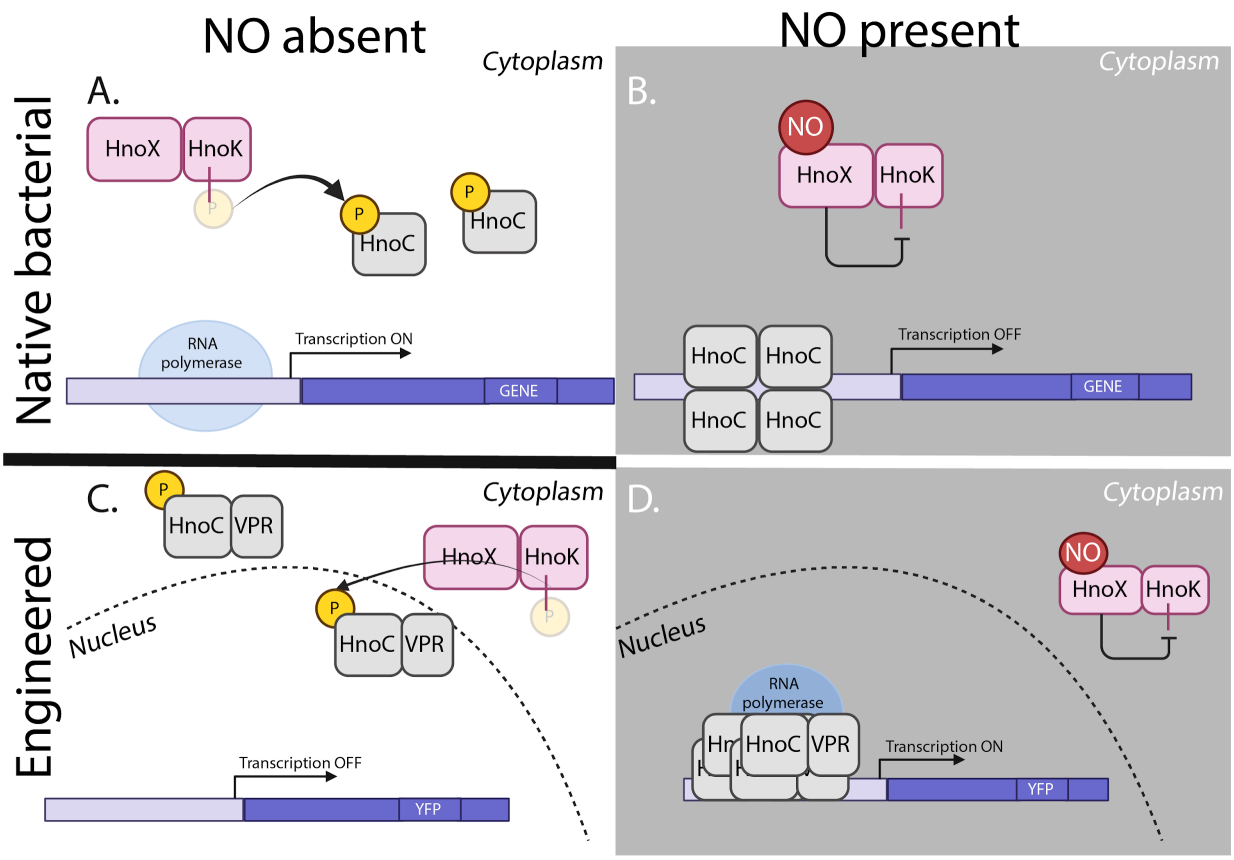

Figure 1. Hno TCS overview. (A) An illustrative schematic overview of the Hno TCS in its native environment in *S. oneidensis* without the presence of nitric oxide (NO), and (B) the formation of an HnoC tetramer that inhibits transcription when NO is present. An illustration of the expected behavior of our engineered TCS pathway with (C) NO absence resulting in no transcription activity due to HnoK activity and (D) increased transcription when NO is introduced.

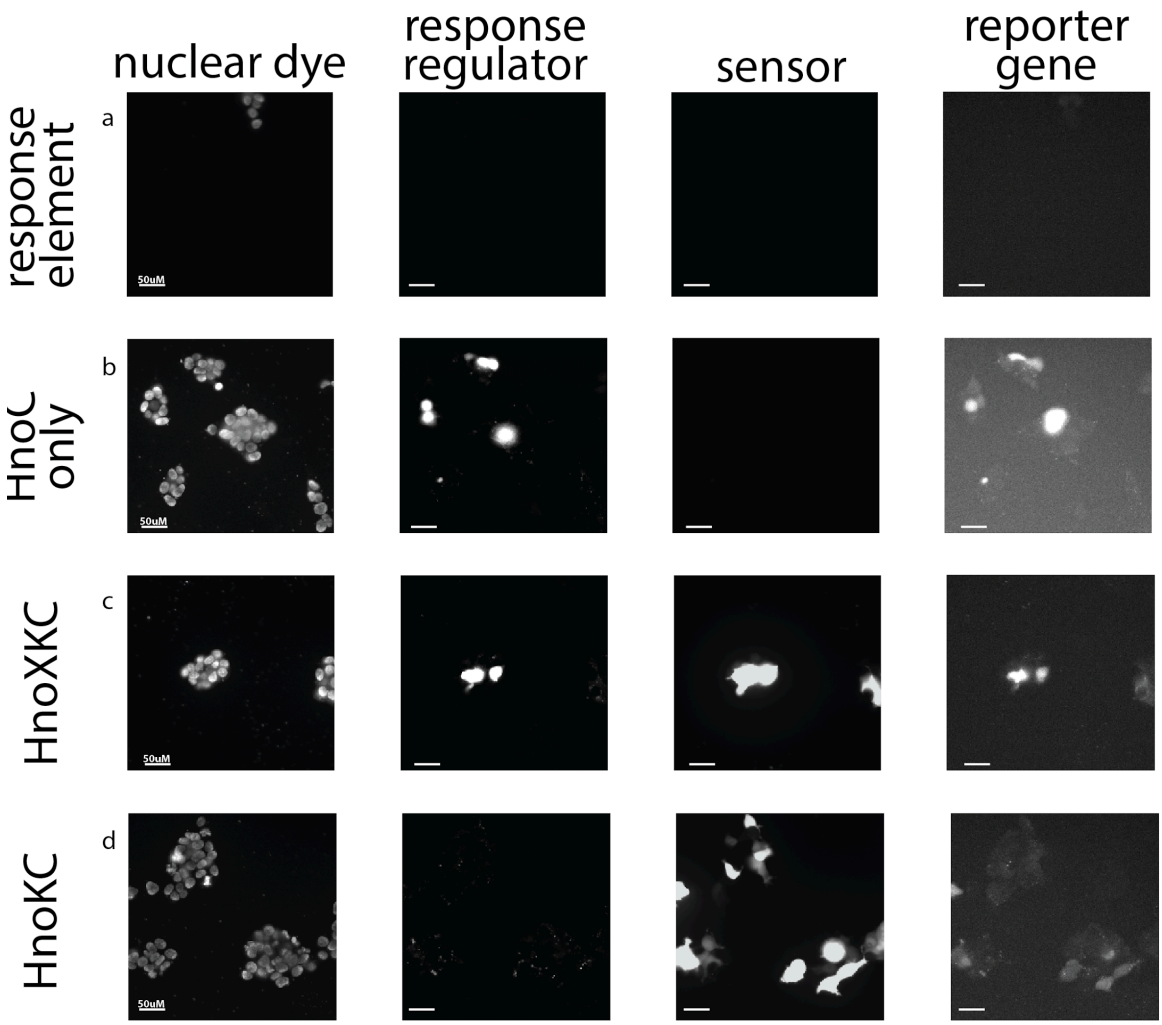

Figure 2. HnoC is sufficient to activate expression of YFP. Representative images of HEK293 cells containing a genomically integrated response element that regulates the reporter gene. These cells were transiently transfected with various combinations of TCS plasmids, each encoding different components of the system. Columns show the signal from different channels imaged at the same time point. Rows represent different conditions of cells with the following components introduced by transient transfection: (A) no TCS components, (B) only HnoC, (C) HnoX, HnoK and HnoC, and (D) both HnoK and HnoC. All cells had the stably integrated reporter gene. Cell images from one day. 50μM scale bar.

Chapter 4

Concluding remarks

Diana Sernas

Department of Microbiology and Molecular Genetics, University of California, Davis, Davis, CA, USA.

4.1 Preface

The contents of this dissertation represent the research that I completed with guidance and mentorship from Dr. Sean Collins. Here I will provide an overview of that research, the tools I contributed, and the knowledge that has been added to synthetic biology in the context of TCS pathways in mammalian cells.

4.2 Discussion and concluding remarks

These studies further support prior work demonstrating that the HKs in TCS pathways retain their ability to phosphorylate their respective RR despite being transplanted into a foreign environment like a cell of a different organism. We were also able to reproduce the ligand independent activation of TCS pathways in mammalian cells. This advances the case for new synthetic biological tools that harness the advantages of TCS including biochemistry that is orthogonal to endogenous mammalian intracellular signaling, the ability to sense soluble ligands, and the potential for wiring different types of outputs. This could pave a novel avenue for cell communication engineering through which researchers could systematically develop strategic signaling cascades in any mammalian cell for their specific research interests. However,

substantial work may still be needed to achieve ligand-regulated TCS pathways in mammalian cells.

In conjunction with previous work, TCS adaptation to mammalian cells has proven difficult even with cytoplasmic sensors. In addition to the HnoXKC and LOV TCS pathways, I considered the Dos pathway, which is sensitive to heme iron (30). The Dos pathway sensor properly localized evenly throughout the cytosol in preliminary results; thus, it may be worth considering in future studies looking for an alternative cytoplasmic pathway. Additionally, we were able to construct the mammalian optimized components for the NarQP TCS, but decided to focus on other pathways, as it responds to soluble nitrate like the NarXL pathway and NarP phosphorylation is a bit less specific than that of NarL (13,31), which I believe can be utilized strategically in future studies to allow for multiple avenues of downstream regulation of the Nar TCS in mammalian cells.

Future studies could optimize the utility of TCS in mammalian cells by testing different combinations of concentrations of components to potentially achieve ligand sensitivity. For instance, these studies with the LOV TCS used high concentrations of each component. In contrast, the Hno studies used transient transfection, resulting in varying levels of expression per component. However, I was not able to overcome technical limitations to ensure enough cells with all components for proper quantification of the Hno results. Perhaps the high expression of each component in the LOV pathway leads to light insensitivity, possibly by diminishing the dynamic range, even with the introduction of the phosphatase promoting components LovR and LovQ. I recommend integrating future HKs under the regulation of a CMV promoter which produces a wide range of expression levels, and systematically comparing light sensitivity at different sensor expression levels.

Additionally, the future of TCS in mammalian cells could possibly be harnessed by skipping wild-type HKs altogether, instead focusing on hybrid sensors. Hybrid sensor proteins are made by fusing the sensor domains of one TCS protein to the signaling domain of another (25). Prior studies (15,25) showed that hybrid TCS sensors retain their ability to phosphorylate their cognate RR. A screen such as the one conducted in Luu *et al.* 2019 (25) could be helpful for systematic identification of sensors with ligand-dependent activity in mammalian cells. While this screen was focused on hybrid sensor expression in bacteria, a screen with hybrid sensors optimized for mammalian cells, especially for immune cells, could help guide investigations for applications in downstream therapeutic applications.

References

1. Marofi F, Motavalli R, Safonov VA, Thangavelu L, Yumashev AV, Alexander M, et al. CAR T cells in solid tumors: challenges and opportunities. Stem Cell Res Ther. 2021 Dec;12(1):81.
2. Sterner RC, Sterner RM. CAR-T cell therapy: current limitations and potential strategies. Blood Cancer J. 2021 Apr;11(4):69.
3. Wang X, Xiao Q, Wang Z, Feng WL. CAR-T therapy for leukemia: progress and challenges. Translational Research. 2017 Apr;182:135–44.
4. Labanieh L, Mackall CL. CAR immune cells: design principles, resistance and the next generation. Nature. 2023 Feb 23;614(7949):635–48.
5. Lim WA, June CH. The Principles of Engineering Immune Cells to Treat Cancer. Cell. 2017 Feb;168(4):724–40.
6. Roybal KT, Lim WA. Synthetic Immunology: Hacking Immune Cells to Expand Their Therapeutic Capabilities. Annu Rev Immunol. 2017 Apr 26;35(1):229–53.
7. Morsut L, Roybal KT, Xiong X, Gordley RM, Coyle SM, Thomson M, et al. Engineering Customized Cell Sensing and Response Behaviors Using Synthetic Notch Receptors. Cell. 2016 Feb;164(4):780–91.
8. Wagner J, Wickman E, DeRenzo C, Gottschalk S. CAR T Cell Therapy for Solid Tumors: Bright Future or Dark Reality? Molecular Therapy. 2020 Nov;28(11):2320–39.
9. Roybal KT, Rupp LJ, Morsut L, Walker WJ, McNally KA, Park JS, et al. Precision Tumor Recognition by T Cells With Combinatorial Antigen-Sensing Circuits. Cell. 2016 Feb;164(4):770–9.
10. Stock AM, Robinson VL, Goudreau PN. Two-Component Signal Transduction. 2000;35.
11. Mascher T, Helmann JD, Unden G. Stimulus Perception in Bacterial Signal-Transducing Histidine Kinases. Microbiol Mol Biol Rev. 2006 Dec;70(4):910–38.
12. Liu C, Sun D, Zhu J, Liu W. Two-Component Signal Transduction Systems: A Major Strategy for Connecting Input Stimuli to Biofilm Formation. Front Microbiol. 2019 Jan 10;9:3279.
13. Hansen J, Mailand E, Swaminathan KK, Schreiber J, Angelici B, Benenson Y. Transplantation of prokaryotic two-component signaling pathways into mammalian cells. Proceedings of the National Academy of Sciences. 2014 Nov 4;111(44):15705–10.
14. Landry BP, Palanki R, Dyulgyarov N, Hartsough LA, Tabor JJ. Phosphatase activity tunes two-component system sensor detection threshold. Nat Commun. 2018 Dec;9(1):1433.
15. Mazé A, Benenson Y. Artificial signaling in mammalian cells enabled by prokaryotic two-component system. Nat Chem Biol. 2020 Feb;16(2):179–87.
16. Chavez A, Scheiman J, Vora S, Pruitt BW, Tuttle M, P R Iyer E, et al. Highly efficient Cas9-mediated transcriptional programming. Nat Methods. 2015 Apr;12(4):326–8.
17. Kawano F, Aono Y, Suzuki H, Sato M. Fluorescence Imaging-Based High-Throughput Screening of Fast- and Slow-Cycling LOV Proteins. Roe AJ, editor. PLoS ONE. 2013 Dec 18;8(12):e82693.
18. Kim H, Willett JW, Jain‐Gupta N, Fiebig A, Crosson S. The *Brucella abortus* virulence regulator, LovhK , is a sensor kinase in the general stress response signalling pathway. Molecular Microbiology. 2014 Nov;94(4):913–25.

19. Swartz TE, Tseng TS, Frederickson MA, Paris G, Comerci DJ, Rajashekara G, et al. Blue-Light-Activated Histidine Kinases: Two-Component Sensors in Bacteria. Science. 2007 Aug 24;317(5841):1090–3.
20. Rinaldi J, Fernández I, Shin H, Sycz G, Gunawardana S, Kumarapperuma I, et al. Dimer Asymmetry and Light Activation Mechanism in *Brucella* Blue-Light Sensor Histidine Kinase. Laub MT, editor. mBio. 2021 Apr 27;12(2):e00264-21.
21. Huynh TN, Noriega CE, Stewart V. Conserved mechanism for sensor phosphatase control of two-component signaling revealed in the nitrate sensor NarX. Proc Natl Acad Sci USA. 2010 Dec 7;107(49):21140–5.
22. Sycz G, Carrica MC, Tseng TS, Bogomolni RA, Briggs WR, Goldbaum FA, et al. LOV Histidine Kinase Modulates the General Stress Response System and Affects the virB Operon Expression in Brucella abortus. Roop RM, editor. PLoS ONE. 2015 May 19;10(5):e0124058.
23. Correa F, Ko WH, Ocasio V, Bogomolni RA, Gardner KH. Blue Light Regulated Two-Component Systems: Enzymatic and Functional Analyses of Light-Oxygen-Voltage (LOV)-Histidine Kinases and Downstream Response Regulators. Biochemistry. 2013 Jul 9;52(27):4656–66.
24. Plate L, Marletta MA. Phosphorylation-dependent derepression by the response regulator HnoC in the *Shewanella oneidensis* nitric oxide signaling network. Proceedings of the National Academy of Sciences. 2013 Nov 26;110(48):E4648–57.
25. Luu RA, Schomer RA, Brunton CN, Truong R, Ta AP, Tan WA, et al. Hybrid Two-Component Sensors for Identification of Bacterial Chemoreceptor Function. Alexandre G, editor. Appl Environ Microbiol [Internet]. 2019 Nov 15 [cited 2021 Dec 2];85(22). Available from: https://journals.asm.org/doi/10.1128/AEM.01626-19
26. Liu N, Xu Y, Hossain S, Huang N, Coursolle D, Gralnick JA, et al. Nitric Oxide Regulation of Cyclic di-GMP Synthesis and Hydrolysis in *Shewanella woodyi*. Biochemistry. 2012 Mar 13;51(10):2087–99.
27. Liu Z, Chen O, Wall JBJ, Zheng M, Zhou Y, Wang L, et al. Systematic comparison of 2A peptides for cloning multi-genes in a polycistronic vector. Sci Rep. 2017 May 19;7(1):2193.
28. Barraud N, Hassett DJ, Hwang SH, Rice SA, Kjelleberg S, Webb JS. Involvement of Nitric Oxide in Biofilm Dispersal of *Pseudomonas aeruginosa*. J Bacteriol. 2006 Nov;188(21):7344–53.
29. Alimoradi H, Greish K, Gamble AB, Giles GI. Controlled Delivery of Nitric Oxide for Cancer Therapy. PNT. 2019 Sep 24;7(4):279–303.
30. Sousa EHS, Tuckerman JR, Gonzalez G, Gilles-Gonzalez MA. DosT and DevS are oxygen-switched kinases in *Mycobacterium tuberculosis*. Protein Sci. 2007 Aug;16(8):1708–19.
31. Darwin AJ, Tyson KL, Busby SJW, Stewart V. Differential regulation by the homologous response regulators NarL and NarP of *Escherichia coli* K‐12 depends on DNA binding site arrangement. Molecular Microbiology. 1997 Aug;25(3):583–95.